Mechanical simulation tool based on impedance matrices

Paolo Ruggi,[1,*] Manuel Pinto,[1] Lucia Trozzo,[2] Giancarlo Cella,[3] Ettore Majorana,[4,5] Giovanni Losurdo,[6,3] Piero Chessa,[7,8] Alessandro Longo,[9,10] and Andrea Viceré[9,10]

[1]*European Gravitational Observatory, Via Edoardo Amaldi, 56021 Cascina (Pisa), Italy*
[2]*Istituto di Fisica Nucleare, Sezione di Napoli, Strada Comunale Cinthia, 80126 Napoli, Italy*
[3]*Istituto Nazionale di Fisica Nucleare, Sezione di Pisa, Largo Bruno Pontecorvo 3, 56127 Pisa, Italy*
[4]*Sapienza Università di Roma, Dipartimento di Fisica, Piazzale Aldo Moro 2, 00185 Roma, Italy*
[5]*INFN, Sezione di Roma, Piazzale Aldo Moro 2, 00185 Roma, Italy*
[6]*Scuola Normale Superiore, Piazza dei Cavalieri 7, 56126 Pisa, Italy*
[7]*Università degli Studi di Perugia, Dipartimento di Fisica e Geologia, Via Alessandro Pascoli, 06123 Perugia, Italy*
[8]*INFN, Sezione di Perugia, Via Alessandro Pascoli, 06123 Perugia, Italy*
[9]*Università degli Studi di Urbino Carlo Bo, Dipartimento di Scienze Pure ed Applicate, Via Santa Chiara, 2761029 Urbino, Italy*
[10]*INFN, Sezione di Firenze, I-50019 Sesto Fiorentino, Firenze, Italy*

(Received 18 October 2024; accepted 18 April 2025; published 8 July 2025)

Octopus is a simulation software specifically developed to calculate the response of a given mechanical system. The initial purpose of its development was to support the design and the commissioning of the superattenuator (SA), i.e., the vibration isolator designed to inhibit the transmission of the seismic noise at the level of the test mass of the Virgo gravitational waves detector. Octopus analytically computes the transfer functions of a complex mechanical system using the impedance matrix formalism in the frequency domain and provides an advanced and versatile mechanical simulation tool. This methodology allows to analyze a large set of user-defined mechanical layouts. Within the context of advanced seismic isolation system design, the present software allows to accurately estimate the behavior of specific mechanical components in terms of performance and general requirements achievement, both in open loop and also when feedback control loops are implemented. In the present work, several topics will be addressed. First, the mathematical principles behind the impedance formalism will be introduced, focusing on the modeling of basic elements, which constitute the principal blocks used to develop and build complex mechanical models. Then, as case studies, two examples of mechanical systems models will be presented: the computation of the thermal noise of a body suspended by an elastic beam and the complete model of a superattenuator. To validate the accuracy of the simulation tool, comparisons with experimental measurements will be given in both cases.

DOI: 10.1103/PhysRevD.112.022002

I. INTRODUCTION

Using an interferometer to detect gravitational waves (GW) requires measuring the variation of the distance between two suspended mirrors (the test masses) [1]. Modern GW detectors, such as Advanced Virgo (AdV) [2], use a Michelson-based interferometer (ITF) with a laser source and two 3 km long Fabry-Perot optical cavities (Fig. 1) to amplify the signal by increasing the optical path traversed by the laser beam. The detector is operated in the so-called dark fringe condition, where destructive interference is achieved between the two beams reflected by the interferometer arms.

Since present interferometers are ground-based, the mirrors must be suspended to a seismic attenuation system. This system must be capable of isolating optical elements from ground seismic motion, so that they can be considered as free-falling bodies above 10 Hz [1,2]. Moreover, the system is designed to steer the optical elements in positions which allow us to reach and stably maintain the working point of the interferometer. The solution adopted in Virgo is a chain of heavy and long pendulums, called superattenuator (SA) [3], see Sec. IV B. The simple working principle based on the properties of the pendulum is combined with a very complex control system, distributed

*Contact author: ruggi@ego-gw.it

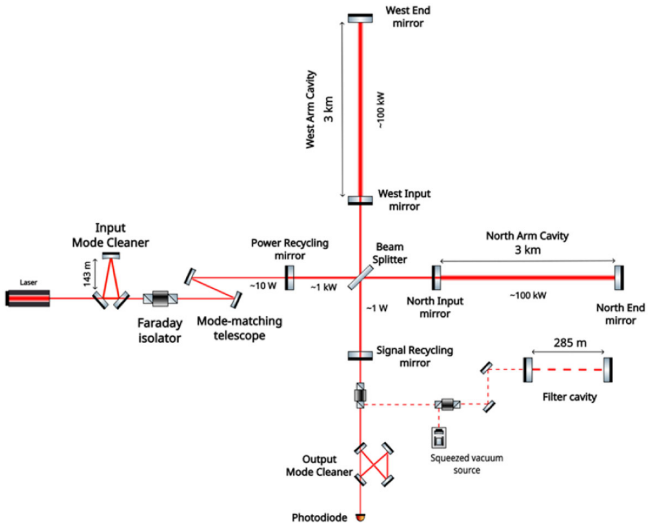

FIG. 1. Optical layout of the AdV + GWs detector.

over many actuation points, in order to achieve a relative root mean square positioning of the test masses at the level of about 10^{-14} m in translation and 10^{-9} rad in angle.

Given the complexity of the GW detectors, the possibility to simulate them accurately, both to predict and understand their behavior, is crucial to guarantee further progress. While a significant effort has been put into optical simulations [4–7], the same cannot be said for vibration isolators and their controls. On the other hand, this aspect is very relevant to get a full understanding of the low frequency noise of the detector, to design optimal control strategies and even to design the hardware of the isolator and to set the requirements. In this paper we present a simulation tool, named Octopus, which has the ambition to fill such a gap and provides an integrated and comprehensive approach to study the problem of isolating a mirror from seismic noise and controlling its position with the required accuracy. This tool has been developed over the last 15 years, helping to analyze the behavior of the SA, design and optimize control strategies, and understand the Virgo noise [8,9]. It is a mechanical simulation software, developed in the Matlab environment, and working in the frequency domain. The tool allows computing the mechanical response, in terms of transfer functions, of a user-defined mechanical system, translating the system description into a set of impedance matrices, which are then combined and solved analytically using the impedance matrix algebra. The main objectives of developing a simulation tool like this are to study the stability and behavior of a mechanical system and its ability to suppress seismic noise, even in the presence of servo-control loops acting on it. These kinds of simulation are challenging from several points of view: they should be able to capture essential features of the system and allow to add details, if needed, in an iterative way. Furthermore, they are intrinsically problematic from a numerical point of view, for the large relative dynamic of their parts. We believe it will mark a significant step forward, also in the perspective of designing the vibration isolation system and its controls for the Einstein Telescope [10]. The code is publicly available in the Zenodo repository [11].

II. TRANSMISSION OF MECHANICAL DISTURBANCES IN FREQUENCY DOMAIN

Under operational conditions, a seismic isolator works in a regime of time invariance and small oscillations. It is therefore legitimate to represent the system using a linear approximation: the variables of motion are outputs of linear operators whose inputs are the forces acting on the system from outside. More in general, the relationship between sets of dynamic variables placed in different points of the chain is always described by a proper linear operator called transfer function (TF). In frequency domain, the TF becomes an algebraic operator in the complex plane of the pulse ω, connecting the Fourier transform of the dynamic variables. In principle, if the Lagrangian of the system is available, the TF is obtained by solving the equations of motion. However, this procedure can be extremely inconvenient to be applied to systems constituted by a lot of bodies with multiple interconnections on different degrees of freedom. An equivalent method has been developed, which requires breaking down the complex system into simple elements. Each element is inserted in the chain by two connection points: input and output. The transmission properties of the element between the two points are assigned by a frequency dependent linear operator, called Impedance, in analogy with the terminology used for the electrical networks. The mechanical impedance of an element, described in Sec. II A, is defined in such a way to be independent on the connection network in which the element is inserted. The connection topology is associated to a set of algebraic formulas (see Appendix A), which allows combining elements and deriving the equivalent impedance of the entire system, for any pair of assigned points in and out. From the impedance, TFs from in to out can be derived as described in Appendix B.

A. Impedance matrix: Definition

In frequency domain, the relationship between a pair of points, in and out, connected by a linear operator, is represented by the square matrix $\mathbb{Z}$:

$$\begin{pmatrix} \boldsymbol{X}_o(\omega) \\ \boldsymbol{F}_o(\omega) \end{pmatrix} = \mathbb{Z}(\omega) \begin{pmatrix} \boldsymbol{X}_i(\omega) \\ \boldsymbol{F}_i(\omega) \end{pmatrix} \tag{1}$$

where $\boldsymbol{X}$ is the collection of the variables of motion (displacement and rotation in space) and $\boldsymbol{F}$ is the collection of conjugate generalized forces (force and momenta coupled from outside). In three dimensions we have three independent displacements $\boldsymbol{x} = (x, y, z)$ and three

independent rotations $\boldsymbol{\theta} = (\theta_x, \theta_y, \theta_z)$ and the conjugate variables are the forces $\boldsymbol{\psi} = (\psi_x, \psi_y, \psi_z)$ and the torques $\boldsymbol{\mu} = (\mu_x, \mu_y, \mu_z)$, so $\boldsymbol{X} = (\boldsymbol{x}, \boldsymbol{\theta})$, $\boldsymbol{F} = (\boldsymbol{\psi}, \boldsymbol{\mu})$ and $\mathbb{Z}$ is a 12×12 matrix.

In the following subsections, some examples of elementary impedance matrices will be presented. [9,12,13] From the examples a detail about the adopted convention will be more clear: $\boldsymbol{F}_i(\omega)$ is applied to the system described by the impedance matrix, $\boldsymbol{F}_o(\omega)$ is applied by the system (so it is minus the applied force).

B. Rigid body

The dynamic of a rigid body, with a mass m and tensor of inertia $\mathbb{J}$, is described by the following system of equations:

$$\begin{aligned} \boldsymbol{x}_o &= \boldsymbol{x}_i \\ \boldsymbol{\theta}_o &= \boldsymbol{\theta}_i \\ -m\omega^2 \boldsymbol{x}_i &= \boldsymbol{\psi}_i - \boldsymbol{\psi}_o \\ -\omega^2 \mathbb{J}\boldsymbol{\theta}_i &= \boldsymbol{\mu}_i - \boldsymbol{\mu}_o \end{aligned} \tag{2}$$

where the two points in and out are coincident with the center of mass. From Eq. (2), the corresponding impedance matrix can be written

$$\mathbb{Z} = \begin{pmatrix} \mathbb{I} & 0 & 0 & 0 \\ 0 & \mathbb{I} & 0 & 0 \\ m\omega^2\mathbb{I} & 0 & \mathbb{I} & 0 \\ 0 & \omega^2\mathbb{J} & 0 & \mathbb{I} \end{pmatrix} \tag{3}$$

where $\mathbb{I}$ is the 3×3 identity matrix. In the simple case of a point mass moving in one dimension, where $\boldsymbol{X} = (x)$ and $\boldsymbol{F} = (\psi)$, Eq. (1) becomes

$$\begin{pmatrix} x_o \\ \psi_o \end{pmatrix} = \begin{pmatrix} 1 & 0 \\ m\omega^2 & 1 \end{pmatrix} \begin{pmatrix} x_i \\ \psi_i \end{pmatrix} \tag{4}$$

C. Elastic element and harmonic oscillator

In an ideal case, an harmonic oscillation of a mass in one dimension is realized when the mass is connected to the ground by a simple elastic mass-less element, only characterized by its stiffness k. The impedance of the elastic element can be derived from the equation connecting the displacement of the two linked points to the applied forces

$$\begin{cases} -k(x_o - x_i) = \psi_i \\ \psi_o = \psi_i \end{cases} \tag{5}$$

which, written in matrix form, gives

$$\begin{pmatrix} x_o \\ \psi_o \end{pmatrix} = \begin{pmatrix} 1 & -1/k \\ 0 & 1 \end{pmatrix} \begin{pmatrix} x_i \\ \psi_i \end{pmatrix} \tag{6}$$

In case of an elastic link involving all the 6 degrees of freedom of a rigid body, the scalar stiffness parameter k needs to be replaced by a generalized 6×6 stiffness matrix and the overall impedance matrix will have dimensions 12×12.

The impedance of the harmonic oscillator can be computed by multiplying the Eqs. (4) and (6) using Eq. (A4), as described in Appendix A, obtaining

$$\mathbb{Z} = \begin{pmatrix} 1 & -1/k \\ m\omega^2 & 1 - m\omega^2/k \end{pmatrix} \tag{7}$$

The 6D oscillation of a rigid body in the space, linked to the ground in its center of mass, can be described by a 12×12 impedance obtained in the same way, using the general version of the respective elementary impedances.

D. Dynamic of a body in gravitational field

The dynamics of a constrained body in a gravitational field, such as a pendulum, cannot be described using the impedance formalism until an additional element is introduced. This element takes into account the effect of a static force $\boldsymbol{T} = (T_x, T_y, T_z)$ associated to the load on a constrained point, when it is separated from the body's center of mass by the vector $\boldsymbol{S} = (s_x, s_y, s_z)$. The six dynamic variable in the center of mass, considered as the input point, are converted in the equivalent variables at the constrained point (output), by the impedance

$$\mathbb{Z} = \begin{pmatrix} \mathbb{I} & -\boldsymbol{S}\wedge & 0 & 0 \\ 0 & \mathbb{I} & 0 & 0 \\ 0 & 0 & \mathbb{I} & 0 \\ 0 & (\boldsymbol{S}\cdot\boldsymbol{T})\mathbb{I} - \boldsymbol{S}\otimes\boldsymbol{T} & \boldsymbol{S}\wedge & \mathbb{I} \end{pmatrix} \tag{8}$$

where $\wedge$ is the cross product and all the elements are 3×3 blocks. The inverse path, from a constrained point to the center of mass, is represented by a similar impedance, with opposite sign both for the displacement and tension.

III. OSCILLATORS IN A GRAVITATIONAL FIELD

The goal of a seismic isolation system is not only to filter ground vibrations but also to keep a test mass in a stable position in all the degrees of freedom very accurately. The pendulum is the key element of a such system. In its simplest representation, it is a point mass suspended from an ideal wire whose horizontal reaction is proportional to its tension. A chain of pendulums is a composite oscillator, and its transfer function can be easily calculated in a simple one-dimensional model. However, in reality, the rotational degrees of freedom of the suspended bodies have a strong

impact on the dynamic of the chain. Indeed, the dynamics of a pendulum are affected by rotations due to the torques applied by gravity and the complex elasticity of a physical link (a massive wire) when acting off-axis. This is typically the case when the pendulum is swinging horizontally. Considering these factors, it is evident that an accurate representation of a multipendulum dynamics can only be achieved by including angular degrees of freedom in the model. The following section will present the impedance matrix of an elastic massive beam, which also includes rotational DOFs.

A. Impedance matrix of an elastic massive beam under tension: Classical solution

The dynamic of an elastic beam, under tension, of length L, is described by the differential equation [12,14]

$$EIx''''(\ell) - Tx''(\ell) = \omega^2 \rho S x(\ell) \tag{9}$$

where $x(\ell)$ describes a small transverse displacement of the beam, which is supposed to be aligned on the z axis. Here E is the Young's modulus, T is the tension, S is the beam cross section, ρ is the material density, I is the momentum of the section, all assumed to be constant along the beam.

There are two independent adimensional parameters which defines the behavior of the beam, a possible choice for them is $\tau = \frac{TL^2}{EI}$ and $\varpi^2 = \frac{\omega^2 SL^4 \rho}{EI}$. These can be used to define a tension dominated regime ($\tau \gg 1$) and an high frequency regime $\varpi \gg 1$. Note that τ can be negative for a compressed beam.

The boundary conditions on the force and momentum are given by

$$\begin{aligned} EIx'''(0) - Tx'(0) &= \psi_x(0) \\ EIx'''(L) - Tx'(L) &= \psi_x(L) \\ EIx''(0) &= -\mu_y(0) \\ EIx''(L) &= -\mu_y(L) \end{aligned} \tag{10}$$

and by choosing $\boldsymbol{X}_i = (x(0), \theta_y(0))$, $\boldsymbol{F}_i = (\psi_x(0), \mu_y(0))$ and $\boldsymbol{X}_o = (x(L), \theta_y(L))$, $\boldsymbol{F}_o = (\psi_x(L), \mu_y(L))$, where $\theta_y = x'$, we can use the general solution of Eq. (9) to connect input and output variables.

We obtain the analytic expression of the beam impedance $\mathbb{Z}_{\text{beam}}$

$$\mathbb{Z}_{\text{beam}} = \begin{pmatrix} \frac{\lambda_+^2 c_- + \lambda_-^2 c_+}{\beta} & \frac{L(\lambda_- s_- + \lambda_+ s_+)}{\beta} & \frac{L^3(-\lambda_+ s_- + \lambda_- s_+)}{EI\gamma^2\beta} & \frac{L^2(c_- - c_+)}{EI\beta} \\ \frac{\varpi(-\lambda_+ s_- + \lambda_- s_+)}{L\beta} & \frac{\lambda_-^2 c_- + \lambda_+^2 c_+}{\beta} & \frac{L^2(c_+ - c_-)}{EI\beta} & -\frac{L(\lambda_- s_- + \lambda_+ s_{+1})}{EI\beta} \\ \frac{EI\varpi(\lambda_+^3 s_- + \lambda_-^3 s_+)}{L^3\beta} & \frac{EI\varpi^2(c_+ - c_-)}{L^2\beta} & \frac{\lambda_+^2 c_- + \lambda_-^2 c_+}{\beta} & \frac{\varpi(\lambda_+ s_- - \lambda_- s_+)}{L\beta} \\ \frac{EI\varpi^2(c_- - c_+)}{L^2\beta} & \frac{EI(\lambda_-^3 s_- - \lambda_+^3 s_+)}{L\beta} & -\frac{L(\lambda_- s_- + \lambda_+ s_+)}{\beta} & \frac{\lambda_-^2 c_- + \lambda_+^2 c_+}{\beta} \end{pmatrix} \tag{11}$$

where $\beta = \sqrt{4\varpi^2 + \tau^2}$, $\lambda_\pm = \sqrt{(\beta \pm \tau)/2}$, and $c_- = \cos\lambda_-$, $s_- = \sin\lambda_-$, $c_+ = \cosh\lambda_+$, $s_+ = \sinh\lambda_+$. This matrix contains all the information describing the dynamics of a real pendulum.

However, it cannot be used in most cases due to the presence of hyperbolic functions. These functions become very large when the beam is a thin and long wire under tension, as is the case with the pendulums used in seismic isolation systems. Their argument λ_+ scales like τ, which is the ratio between the total length L and the bending length EI/TL. This is typically ≈ 100, making the typical value of the impedance element $\approx e^{100}$.

B. Impedance matrix of an elastic massive beam under tension: Octopus's solution

A solution of the numerical problem affecting the beam impedance has been proposed in [9] and used for a long time. It consists in connecting a virtual spring in parallel to the beam. The spring has a longitudinal stiffness ϵ and an angular stiffness k_θ. It is represented by the following 4×4 matrix $\mathbb{Z}_{\epsilon,k_\theta}$.

$$\mathbb{Z}_{\epsilon,k_\theta} = \begin{pmatrix} 1 & 0 & -\frac{1}{\epsilon} & 0 \\ 0 & 1 & 0 & -\frac{1}{k_\theta} \\ 0 & 0 & 1 & 0 \\ 0 & 0 & 0 & 1 \end{pmatrix} \tag{12}$$

The parallel connection between the matrices expressed by Eqs. (11) and (12) is calculated using Eq. (A5). The new impedance matrix $\mathbb{Z}'_{\text{beam}}$ depends on the parameters of the virtual spring ϵ, k_θ, and on the only hyperbolic function $\tanh\lambda_+$, which is equal to 1 when the value of the argument is large ($\lambda_+ > 10$). Making the limit around the point $\lambda_+ \to \infty$ of $\mathbb{Z}'_{\text{beam}}(\epsilon, k_\theta, \tanh\lambda_+)$ and then sending $\epsilon \to 0$, it is possible to derive the analytic expression of the impedance $\mathbb{Z}_{\text{beam},k_\theta}$

$$\mathbb{Z}_{\mathrm{beam},k_\theta} = \begin{pmatrix} \frac{\varpi}{\lambda_+^2 s_-} + c_- + \frac{EI\varpi^2}{Lk_\theta\lambda_+^3} & \frac{L(\beta+2\varpi s_- +\tau c_-)}{\beta\lambda_+} + \frac{EI}{k_\theta} & \frac{L^3(2c_- - \frac{\tau s_-}{\varpi})}{EI\beta\lambda_+ + \frac{L^2}{\lambda_+^2 k_\theta}} & -\frac{L}{\lambda_+ k_\theta} \\ \frac{\varpi^2 EI}{\lambda_+^2 L^2 k_\theta} & \frac{EI\lambda_+}{Lk_\theta} + 1 & \frac{L}{\lambda_+ k_\theta} & \frac{1}{k_\theta} \\ \frac{EI\varpi\beta s_-}{L^3\lambda_+} + \frac{EI^2\varpi^4}{L^4\lambda_+^4 k_\theta} & \frac{EI\varpi}{L^2}\left(s_- + \frac{(1-c_-)\varpi}{\lambda_+^2}\right) + \frac{EI^2\varpi^2}{L^3\lambda_+ k_\theta} & \frac{\varpi}{\lambda_+^2 s_-} + c_- + \frac{EI\varpi^2}{Lk_\theta\lambda_+^3} & -\frac{\varpi^2 EI}{\lambda_+^2 L^2 k_\theta} \\ -\frac{EI\varpi}{L^2}\left(s_- + \frac{(1-c_-)\varpi}{\lambda_+^2}\right) - \frac{EI^2\varpi^2}{L^3\lambda_+ k_\theta} & \frac{EI(-2\beta\lambda_+^2 + 2\varpi^2 c_- - \varpi\tau s_-)}{L\beta\lambda_+} + \frac{EI^2\lambda_+^2}{L^2 k_\theta} & -\frac{L(\beta+2\varpi s_- +\tau c_-)}{\beta\lambda_+} - \frac{EI}{k_\theta} & \frac{EI\lambda_+}{Lk_\theta} + 1 \end{pmatrix} \tag{13}$$

The new impedance describes a mechanical system equivalent to the bare beam, with the exception of a small additional coupling, due to the added angular spring that can be set small enough to affect just the low frequencies.

The distortion affects a smaller frequency band as the value decreases. Normally the distortion can be limited below 1 mHz, out of the interesting range for the common studies involving mechanical simulations. The amplitude of the elements in the new impedance is not as large as in the Eq. (11). Its use does not induce any numerical instability and gives exactly the same results.

C. Frequency response of the simple pendulum

The impedance of a simple pendulum, from the suspension point to the center of mass (c.m.) of the suspended body, is given by

$$\mathbb{Z} = \mathbb{M}\mathbb{S}\mathbb{Z}_{\mathrm{beam}} \tag{14}$$

Eq. (14) is the result of the series connection [Eq. (A4)] of these three elements:

(i) the suspension wire $\mathbb{Z}_{\mathrm{beam}}$, Eq. (13);
(ii) the element $\mathbb{S}$, Eq. (8), containing the information about the connection point between the wire and the rigid body;
(iii) the rigid body $\mathbb{M}$, Eq. (3)

The impedance (14) is calculated for one horizontal displacement and the rotation around the orthogonal direction: M and S are reduced to 4X4 submatrices associated to the corresponding coordinates. The tensor of inertia is reduced to the scalar value associated to the rotational axis. The explicit expression of $\mathbb{S}$ is

$$\mathbb{S} = \begin{pmatrix} 1 & s_y & 0 & 0 \\ 0 & 1 & 0 & 0 \\ 0 & 0 & 1 & 0 \\ 0 & -s_y T_y & s_y & 1 \end{pmatrix} \tag{15}$$

Given that the wire is vertically oriented and the connection point must stay on the vertical axis passing through the c.m., both T and s are defined by the vertical coordinate only.

The 2X2 frequency response to a force or a torque applied to the body is given by Eq. (A22) and contains also the information of the cross-coupling between translation and rotation. The result is shown in Fig. 2 for two cases: the link is in the c.m. ($s_y = 0$); the link is below the c.m. In the second case, the elastic reaction of the wire to a rotation is partially compensated by the effect of the gravity, because the c.m. tends to fall. The resonant frequency of the rotation decreases as s_y increases and the same happens for the cross-coupling terms, until the system becomes unstable and the resonance disappears for too large values of s_y. Figure 3 shows the longitudinal TF of a pendulum from the suspension point to the suspended mass, over a large range of frequency. The transmission of vibration is amplified at high frequency by the internal resonances of the wires. The effect is determined by the mass, the elasticity and the tension of the wires.

It is interesting to note that if we evaluate analytically the transfer functions from (14) we find a well defined results in the limit $EI \to 0$, also by using the impendence $\mathbb{Z}_{\mathrm{beam}}$ and there is no need to introduce the regularized one $\mathbb{Z}_{\mathrm{beam},k_\theta}$. For example the transfer functions between a

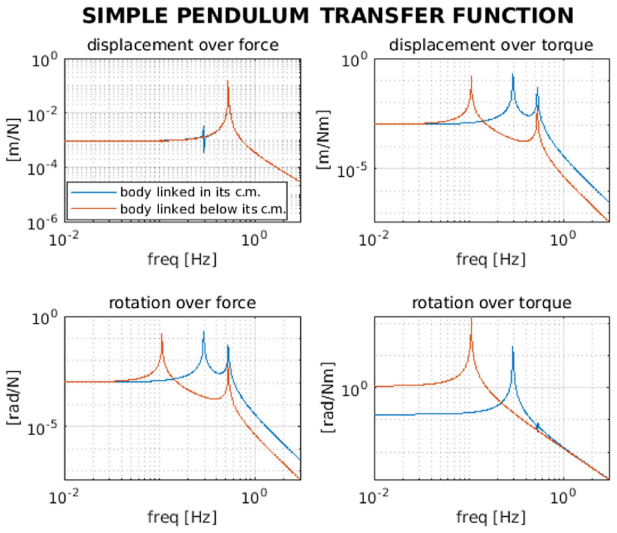

FIG. 2. Transfer function between displacement/rotation and force/torque for a simple pendulum—a rigid body weighing 100 kg, hanging from a steel wire 0.9 m long and 1.5 mm thick. The blue trace refers to the case of a body linked to the wire in its c.m. The red trace refers to the case of a body linked to the wire 6 mm below its c.m.

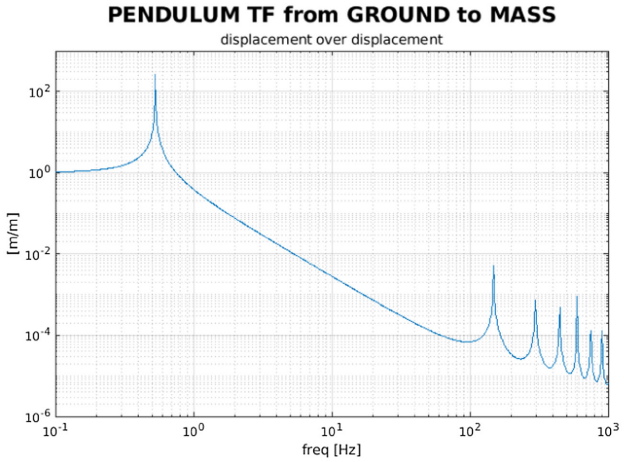

FIG. 3. Pendulum transfer function from ground displacement to suspended mass displacement. The internal resonances of the suspension wires produce the characteristic peaks at high frequency, known as violin modes. This effect is perfectly described by the model because the impedance includes the mass ad elasticity distribution along the wire.

displacement of the suspension point and the displacement of the mass are given by

$$\lim_{EI\to 0} TF(X_i, X_o) = \begin{pmatrix} \frac{\omega_p^2}{\omega_p^2 \cos\left(\gamma\frac{\omega}{\omega_p}\right) - \frac{\omega_p}{\gamma}\omega \sin\left(\frac{\gamma}{\omega_p}\omega\right)} & 0 \\ 0 & 0 \end{pmatrix} \quad (16)$$

where $\gamma^2 = \rho SL/m$ is the ratio between the wire's mass and the rigid body's one, $\omega_p^2 = g/L$, we approximated $T = mg$ neglecting the mass of the wire and we set $s_y = 0$ for simplicity. In this limit the flexural stiffness of the wire is zero and angular variables are completely decoupled. When $\gamma \to 0$ we obtain a simple pendulum, while in the general case we observe all the peaks related to the internal resonances of the wire.

This results clarify that the problem cured by the regularized $\mathbb{Z}_{\text{beam},k_\theta}$ is entirely computational. It is not practically possible to manipulate symbolically the impedence arrays of a complex system to get the transfer functions and we need to evaluate them numerically first.

D. Modeling links in Octopus

The impedance of an elastic beam is extensively used in Octopus: in addition to describing the simple pendulum, it is also the basic element of complex links, like inverted pendulum, cantilever blades and centering systems. The code provides functions returning the impedance of those links, based on their technical drawings, along with some free parameters that the user must define. Complex configurations can be built (see Appendix B), including any number of links among the objects available in the library. An example is shown in Fig. 4: a mass suspended to 4 equal wires in a symmetrical configuration, as it happens for the test masses used in GW detectors. Each wire is linked to the upper and lower body in a point specified by the vector s, which stores the coordinates of the point with respect to the c.m.

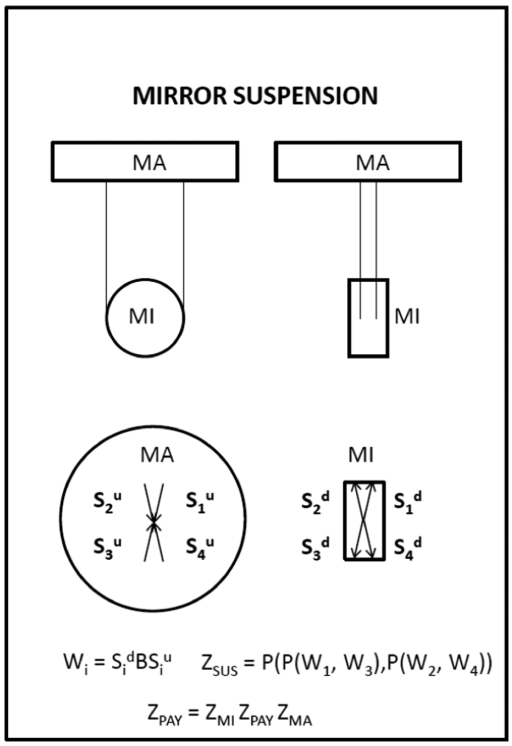

FIG. 4. Schematic representation of a link composed by multiple wires.

IV. MODELS VALIDATION

To validate the accuracy of the simulation tool, the comparison between the simulated transfer functions and those measured experimentally for a given mechanical system will be shown. In this section, two cases are presented. In Sec. IV A we evaluate the thermal noise of a body suspended by an elastic beam. In Sec. IV B we will model a complete AdV + Super Attenuator.

Concerning the SA, mechanical data will be exploited to build the model, including also the implementation of an accelerometer sensor as a material object. The simulation results will be compared to different experimental measurements carried out in 2018.

A. The thermal noise of a body suspended by an elastic beam

In statistical physics, thermal noise refers to all fluctuations present in a physical observable of a macroscopic system that is in thermal equilibrium with the external environment [1].

In the case of a mechanical system the spectral density $x^2(\omega)$ of the thermal fluctuations of the observable $X_p(\omega)$

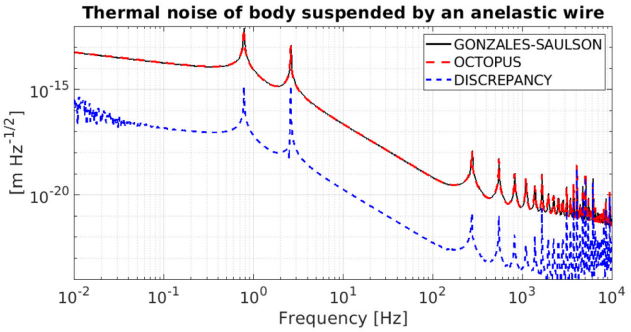

FIG. 5. Comparison between the amplitude spectral densities for the thermal noise estimated by Saulson-Gonzàlez [16] (black curve) and that estimated using Eq. (17) (red curve). Blue dashed curve represents the relative discrepancy between the two results.

is related through the fluctuation-dissipation theorem [15] to the transfer function $H(\omega) \equiv X_p(\omega)/(F_p(\omega)$ between X_p and a force F_p coupled to it

$$x^2(\omega) = \frac{4k_B T_s}{\omega} \mathrm{Im}\, H(\omega) \tag{17}$$

Here k_B is the Boltzmann constant, and T_s is the absolute temperature of the system.

To assess the accuracy of Octopus in reproducing results, the thermal noise of a mechanical system, having the same properties of the system described in [16], is calculated using Eq. (17). This equation requires the $H(\omega)$ transfer function, which is calculated with our tool.

The system under consideration consists of a rigid body with a mass of m that is connected to the ground by an elastic wire. Within the Octopus environment, it can be represented by a node of impedance $\mathbb{Z}$, which is a combination of the impedance of the rigid body [Eq. (3)] and the impedance of the wire [Eq. (13)]. Once the $\mathbb{Z}$ of the system is known, Eq. (A22) can be used to calculate $H(\omega)$ and subsequently determine the thermal noise of the system. Figure 5 shows the amplitude spectral densities for the thermal noise derived from Gonzàlez and Saulson in their paper [16] (black curve) and that estimated using the Octopus transfer function (red dashed curve). It can be seen that the two calculation methods give the same result with a relative discrepancy of about 10^{-3} (blue dashed curve).

B. The Virgo superattenuator

The Virgo SA is a cascade of seven pendulums plus a soft preisolation stage (inverted pendulum). Length of the suspension wires between the stages is chosen in order to have the principal modes of the chain confined below 2 Hz (neglecting the internal modes of elastic elements such as wires). The system acts as a passive mechanical filter [17]. At larger frequencies, a steep transfer function from the ground to the suspended element provides a large passive attenuation already at 4 Hz.

The support for the suspension point of the pendulums chain is a three-leg mechanical structure operating on the inverted pendulum (IP) principle [18]. A fine tuning of mass and stiffness allows a setting of the IP resonance at 30 mHz.

In the final stage, known as the payload, the optical element is suspended by four fused silica wires from a steering element called marionette. At this stage, a high mechanical precision and a very low level of dissipation are required in order to guarantee perfect positioning and minimal vibration. The double pendulum is surrounded by an heavy upper stage, supporting actuators and additional optical devices. Figure 6, left side, shows the CAD drawing of the SA with the details of the main elements composing the structure; on the right side, the correspondent scheme, representing the physical layout of the system, is shown.

In order to actively control the SA and the payload elements in their correct working points, the whole structure is provided of specific sensing and driving elements. Feedback controls are applied at the top stage (IP and F0), the Filter7 (F7)-marionette stage, and the test mass (mirror) (refer to Fig. 7).

The main requirement of the control strategy of the superattenuator is to keep the IP and the whole suspended optical elements within a fixed range around the working point, in order to damp the main resonances of the suspension chain, filter the seismic disturbances transmitted from the ground to the test masses, and so to reduce the needed dynamic range of the actuators for the locking control of the test masses. On these bases, the control of the superattenuator is based on the so-called *hierarchical control strategy*, which divides the frequency band of

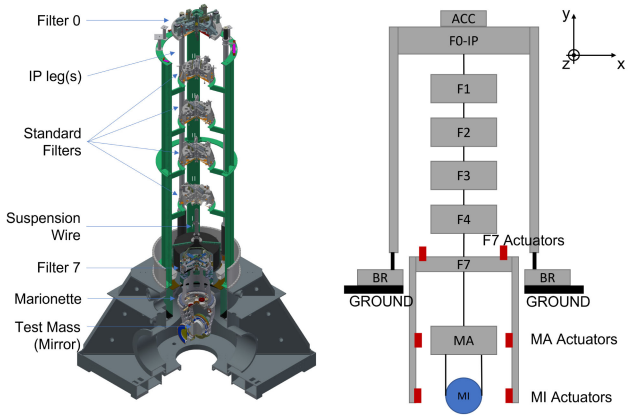

FIG. 6. SA CAD drawing (left) and the correspondent schematic representation (right). The system is composed by a test mass (MI) suspended from a marionette (MA) via four silica wires. The marionette is suspended from Filter7 (F7) by a maraging steel wire. A chain of five standard filters starts from F7 and ends with Filter1 (F1). Each filter is suspended to the others also through a maraging steel wire. F1 is connected to the preisolator (F0 + IP), connected to ground via the bottom ring (BR).

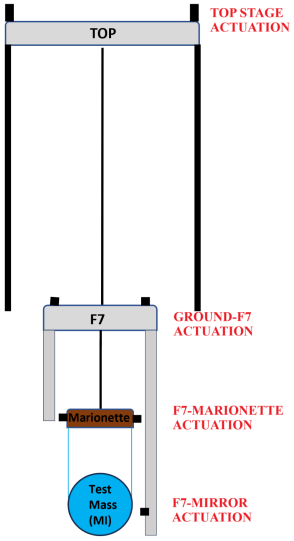

FIG. 7. Schematic view of a SA where the actuation points (Top-stage, F7-marionette, and F7-mirror), are put in evidence.

correction force along the different level of actuation points: IP, test mass and marionette. At the level of the top stage, actuators which allows higher dynamics are used. The consequent higher noise is filtered down to the test mass through the mechanical filters along the chain. Thus, at the level of the mirror, the achieved attenuation allows to use for the locking low-noise actuators with less dynamics and consequently to increase the frequency band of actuation.

At the top stage level (F0), the inertial damping (ID) control loop of the inverted pendulum is implemented. The strategy of the IP inertial control is based on the idea of taking the best information out of the available sensors, which are position sensors, the LVDT (linear variable displacement transducer) and the accelerometer, respectively. In AdV + SA, three accelerometers for the horizontal degrees of freedom and two for the vertical are distributed along the top stage of the inverted pendulum. The top stage is provided of three position sensors for the horizontal degrees of freedom and one for the vertical. LVDT and accelerometer sensors are connected to the IP, measuring its relative motion with respect to the ground and the suspended mass of the accelerometer, respectively, producing a force to be applied to the IP in order to damp the principal resonance modes of the system [19–21]. Experimentally we find that, typically, below 100 mHz we are limited by the sensing noise of the accelerometer, while above such frequency range we are limited by the LVDT sensing noise. Thus, in the development of the IP inertial control, a control loop is built with the aim of reducing the coupling with seismic motion through the use of the in-loop position sensors connected to ground, using an error signal which is not affected by such disturbances in the whole band of control. This is done through the so-called blending strategy, which is a technique that takes the sum of the two signals coming from the LVDTs and the accelerometers, conveniently prefiltered through the use of dedicated filters, i.e., a low-pass and a high-pass, respectively. The shaping of the blending filters and the crossing frequency, are conveniently designed based on a trade-off in order to filter the reinjection of seismic noise through the position sensor above 100 mHz and the reinjection of tilt noise below 100 mHz through the use of the accelerometer, respectively. An additional actuation point is located at the level of filter 7. Displacement sensors and magnetic coil actuators are installed at this level, with a purpose to both monitor the displacement of filter 7 and to dampen the torsional mode of the chain. A set of optical levers and voice coil actuators is installed at the marionette and the test mass. These are used to monitor and dampen the test mass's angular degrees of freedom (pitch, yaw, and roll) and to steer the test mass to the optimal position to reach the detector operating point.

C. SA transfer functions: Simulations vs experimental data

Octopus models of SA have been built as described in Appendix B 1, using technical data from AdV + suspensions. The results of the simulation have shown good agreement with a detailed experimental characterization. Experimental data provide transfer functions (see Appendix A 2) of the motion between points where displacement sensors are located, or the response to forces applied in the points where actuators are located. In an Octopus model, sensing and actuation points are identified as NODES (see Appendix B 1), having well defined spatial coordinates. In case of internal actuation (from one to another body of the suspension), a specific node is added on the actuation cage. In this way, the simulation can take into account at the same time the force applied to the controlled body and the recoil of the actuation cage.

In the following, simulation results for several open-loop transfer functions of the modeled SA are reported. The simulations that will be shown, have been computed in the frequency range from 10^{-2} Hz up to few tens of Hz.

In order to calibrate in the same measurement units both the simulations and experimental measurements, real actuator gains values have been taken into account to switch to the m, N, rad units system. The chosen coordinate system is the one reported in the right scheme of Fig. 6. This is analogous to the real reference system used in AdV+, where the z direction is the longitudinal one that coincides with the direction of the arm and optical axis. In Fig. 8, mechanical plants of the IP are shown. In details, the case of the displacement of the top stage F0 for a given force or torque applied to the same point is investigated; three horizontal degrees of freedom have been simulated: transversal, longitudinal and rotational along the vertical axis, i.e., X, Z and TY respectively.

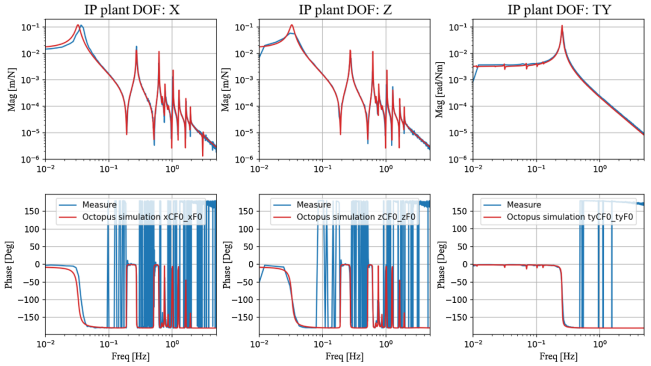

FIG. 8. Comparison between measurement (blue trace) and model (red trace) of the mechanical plant of the IP. Horizontal degrees of freedom have been considered: transversal (X), longitudinal (Z), torsional (TY).

In the blue traces, experimental measurements are reported, while in the red traces the comparison with Octopus simulations are given.

As shown, simulation results are in good agreement with the performed measurements. In the X and Z cases, one can notice how the system behaves symmetrically. All the mechanical resonances of the filter stages composing the pendulum chain are visible, together with the correspondent phase sign flip; in the rotational DOF (Yaw), only the principal angular resonance frequency is visible.

Another interesting scenario which has been investigated is the mechanical transmission of the seismic motion through the IP, in which one can appreciate the role of the IP as a passive mechanical attenuator.

Comparison between model and measurement is reported in Fig. 9: the longitudinal Z DOF has been considered. Simulation has been done by setting as output the IP longitudinal displacement imposing an input displacement of the reference ground. The simulation result is well in agreement with the measurements, in the region where the pendulum resonances make the transmission larger. Above 2 Hz the transmitted motion is quite small because the shaking in input is just the ground motion and the transfer function is small: the measurement is less reliable. Starting from about 10 Hz the flexural modes of the IP legs and other internal modes of the complex top stage structure become dominant in the transmission. The model can only reproduce the legs resonance because the top stage is considered as a rigid body. The visible discrepancies are therefore somehow expected.

Figure 10 shows the force to displacement transfer function between the IP and F7 when a longitudinal force is applied to the IP. The experimental measurements are represented by the blue trace, while the result of the Octopus simulation is shown by the red trace. Both simulated and measured transfer functions clearly show the modes of the system. Starting from the lower frequencies, the two fundamental longitudinal modes of the system can be identified. The first mode, at about 30 mHz, is the IP mode, and the second, at about 250 mHz, is the main pendulum chain mode. In Fig. 11, the recoil effect of the F7 due to a longitudinal actuation on the marionette is shown. In details, the angular response of F7 around the Z axis, due to an actuation on the marionette along the horizontal X axis is reported on the left subplot. In the right subplot, the analogous scenario, with the angular response of the F7 around the x axis, for a longitudinal actuation on marionette along the Z direction is reported. As shown, within the frequency region in which the measurement is good, the agreement between measurement and model is good, as an indication that the simulation is able to accurately reproduce dynamics in which complex couplings, such as

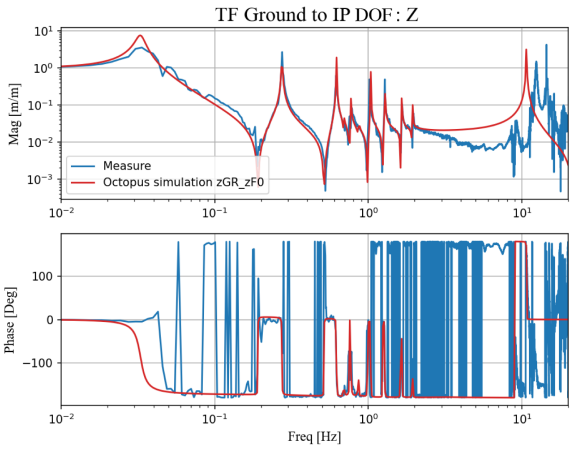

FIG. 9. Comparison between measurement (blue trace) and model (red trace) of the seismic motion transfer through the IP. The first resonance around 30 mHz and partially the one above 10 Hz can be ascribed to the own modes of the IP, while the peaks between are related to the filter chain below.

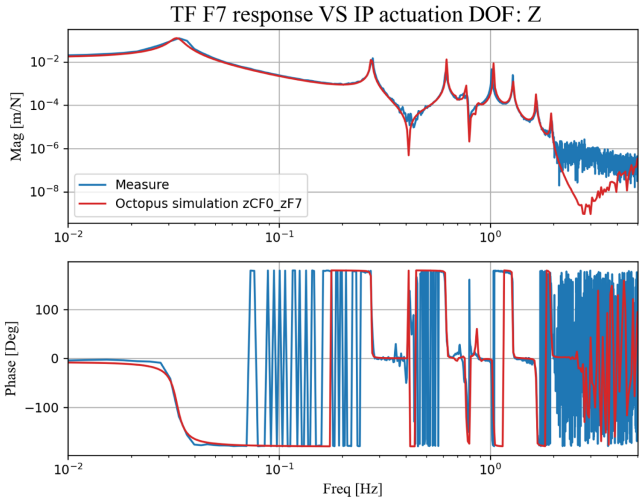

FIG. 10. Comparison between measurement (blue trace) and model (red trace) of the F7 response for a given force applied on the IP along the Z DOF.

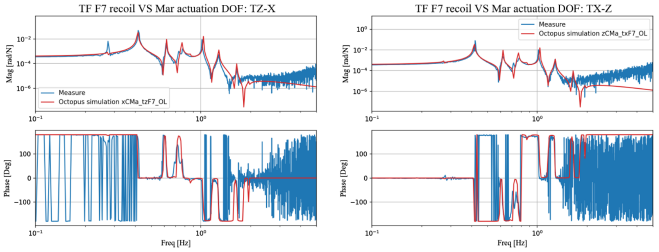

FIG. 11. Comparison between measurement (blue trace) and model (red trace) of the F7 recoil for a applied force on X DOF of the MA (left) and Z DOF of the MA (right).

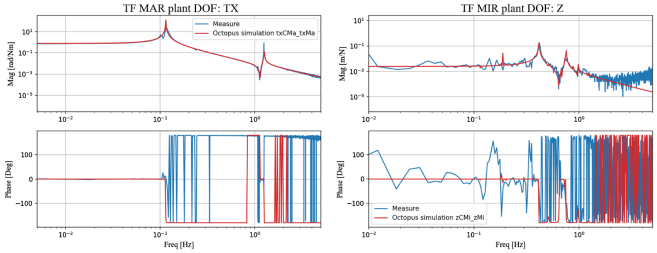

FIG. 13. Comparison between measurement (blue trace) and model (red trace) of the mechanical plant of the marionette TX DOF (left) and Z DOF of the MI (right).

longitudinal to angular, are involved. One last set of transfer functions are here presented, which are the angular mechanical plants of the F7 and the marionette, and the longitudinal mechanical plant of the test mass. In details, the chosen degrees of freedom for this set of transfer functions are yaw (TY) for the F7, pitch (TX) for the marionette and Z for the test mass. Figure 12 shows the mechanical plant of F7 in which the Yaw DOF (TY) is considered. Both simulated and measured transfer functions show the torsional mode of the chain at about 12 mHz.

In the left plot of Fig. 13 is reported the mechanical plant of the marionette, in which the pitch DOF (TX) is considered. Such plants are the ones used to build the so called angular local controls to control the mirror orientation, in the local reference system, using the error signal coming from the marionette's optical lever sensing.

As shown in the plots, also in the present case the model reproduces perfectly the experimental measurement.

As last example in the right subplot of Fig. 13, the longitudinal (Z) test mass mechanical plant is reported. In the specific case, this mechanical plant is the one used to control the most important longitudinal degree of freedom,

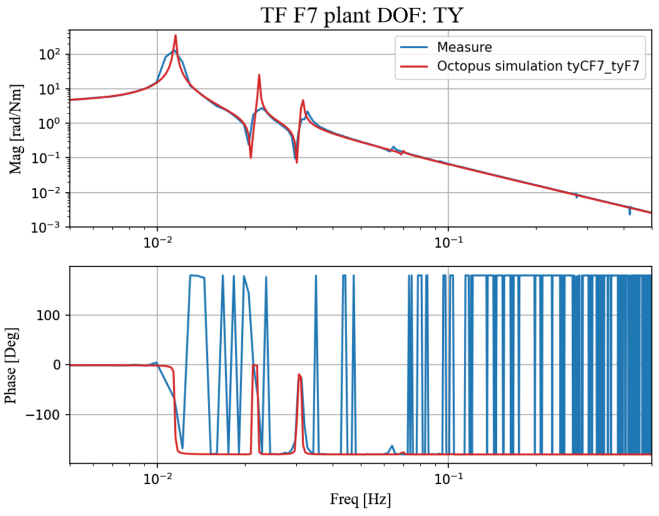

FIG. 12. Comparison between measurement (blue trace) and model (red trace) of the mechanical plant of the F7 torsional DOF (TY).

which is related to the longitudinal Fabry-Perot cavity length, i.e., differential arm length (DARM).

In the simulation results reported in the red trace, the principal resonance frequencies of the pendulum (at around 0.4 and 0.8 Hz respectively) are visible. These values are confirmed by the measurements, although noisy, reported in the blue trace.

The previously shown mechanical plants (IP, F7, MAR, and MIR) introduce the possibility of implementing feedback control loops. The working principle of the control implementation in Octopus is based on the creation of a connection between two nodes among which the sensing and the actuation is performed. This connection allows to compute a specific impedance matrix which assumes the role of an equivalent frequency-domain stiffness. Values of this matrix depend on the shape of the controller: the outcome is a resulting force to be applied to the system for a given displacement of the controlled subsystem. Details of the implementation of a feedback control loop are presented in Appendix C.

We conclude this section showing an example of the effect of the implementation of a real feedback control loop, i.e., the inertial damping (ID) of the inverted pendulum. The control architecture of the ID is based on the blending strategy briefly introduced in Sec. IV B. In Fig. 14 is shown the response of the IP to the transmission of the seismic motion when the inertial damping control is active. In details, in the green trace is reported the simulated transfer function in open-loop representing the passive transmission of the seismic motion to the IP (already presented in Fig. 9); in the red trace the simulated IP residual motion in closed-loop is shown, while in the blue trace, the comparison of the closed-loop response with the experimental data is given.

One can appreciate the attenuation effect of the controller toward the principal resonance modes of the chain. Just above the IP resonance frequency (30 mHz), the transmission of seismic motion is increased by the loop because a ground-based sensor needs to be used in place of the inertial sensor at low frequency. The shape of the transfer function follows the shape of the low-pass filter applied to the position sensor and depends on the strategy of blending between position and inertial sensing. The complex effect of sensor properties and filtering strategy is well

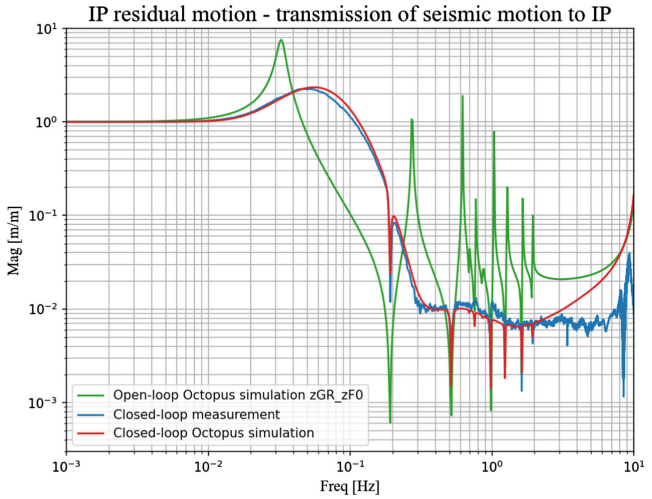

FIG. 14. Inverted pendulum residual motion: transmission of the seismic motion to the IP with inertial damping control active. Green trace: simulated passive seismic transmission (open-loop); Red trace: simulated residual motion of the IP (closed-loop); Blue trace: measured residual motion of the IP (closed-loop).

reproduced by the simulation. The discrepancy above a few Hz can be ascribed to the difficulty of having a reliable measurement of the residual seismic motion downstream the suspension.

Given the latter examples, both in open-loop and closed-loop, we can highlight the powerful properties of Octopus also as a control designing tool, as it is done in the real applications. Indeed, starting from the mechanical plants of a given system, it is possible to design and test proper feedback controllers, which allows to evaluate the performance of a mechanical system in closed-loop in terms of stability, residual motion of the main elements, hardware noise projection, and general requirements achievement.

V. CONCLUSIONS

Impedance matrices are a powerful representation of multidimensional mechanical systems in the frequency domain, allowing the point-to-point transmission of disturbances to be derived from the algebra of connections. However, the implementation of an efficient simulation tool based on this method is not feasible if the standard impedance of the elastic beam is used. In fact, this impedance contains elements that are too large, reducing the accuracy of any calculation derived from it. To address this issue, within this work a solution has been presented to convert this impedance into another that is almost equivalent, but avoids computational problems and makes any simulation tool accurate.

The impedance method has been used to develop and test a Matlab code called Octopus over several years. The mechanical simulations developed in Octopus include control loops. To prove its efficiency, results which are supported by both theoretical and experimental data have been presented.

Given the good match between experimental data and Octopus results, it is possible to assert that the transfer functions computed with this tool can be used to evaluate the transmission properties of a seismic isolation system, mechanical plants of controlled systems, control system performance, and in-loop residual motion of suspended mass for given external disturbances and control noises. This information is crucial for deriving requirements and driving the development of seismic isolation systems for advanced GW detectors.

ACKNOWLEDGMENTS

The research activity of L. T. is partially funded by the "PNRR ETIC IR0000004, "EINSTEIN TELESCOPE INFRASTRUCTURE CONSORTIUM" – CUP I53C21000420006 MISSIONE 4, COMPONENTE 2, INVESTIMENTO 3.1 - Fondo per la realizzazione di un sistema integrato di infrastrutture di ricerca e innovazione". The research activity of A. L. is partially funded by the European Gravitational Observatory under Contract No. EGO-0262-A-24. The research activity of P. C. is partially funded by Ministero dell'Università e della Ricerca (MUR-Italy) under the Contract LoVec ET PRIN2020 and through the program "Dipartimenti di Eccellenza 2018-2022" (Grant SUPER-C), the European Gravitational Observatory under the Contract No. EGO-DIR-44-2022, INFN under the Einstein Telescope Infrastructure Consortium (ETIC - IR0000004) PNRR M4, C2, Investimento 3.1.

DATA AVAILABILITY

No data were created or analyzed in this study.

APPENDIX A: ALGEBRAIC RULES OF THE IMPEDANCE MATRICES

This section presents algebraic rules for linking impedance matrices and additional rules for deriving transfer functions from impedances.

The impedance matrix framework requires the decomposition of a complex mechanical system into simpler subsystems, each one associated with its own impedance. Within this framework, any connection scheme between subsystems can be expressed in terms of algebraic rules between corresponding matrices. Once two points of the system are selected as input and output, the net of impedances and connections can be reduced to a single impedance matrix (Z). This matrix will contain all the information about the transmission of mechanical perturbations from in to out.

In order to define a set of useful algebraic formulas, the 12×12 matrix Z needs to be expressed in terms of four 6X6 submatrices, A, B, C, D

$$Z = \begin{pmatrix} A & B \\ C & D \end{pmatrix}. \tag{A1}$$

In the real systems, the four submatrices are not totally independent: they are normally compliant with the following identities

$$AD^T - BC^T = I \quad AB^T = BA^T \quad CD^T = DC^T \tag{A2}$$

As (A2) are true for all the representations of elementary systems used in Octopus, and as all the connections used in Octopus maintain the identities, we can conclude that the representation of complex systems derived in Octopus are compliant with the identities. A notable exception is the case of a charge in an external magnetic field where

$$Z = \begin{pmatrix} I & 0 \\ i\omega q\mathbf{B} \wedge & I \end{pmatrix} \tag{A3}$$

which violates $CD^T = DC^T$.

Representations of some active control systems are also an exception. For the derivation of the closed loop transfer function, normally the aforementioned identities cannot be used.

1. Reduction of a complex mechanical system to a single impedance system

Let us consider two systems S_1 and S_2, connected one to the other and represented by the impedances Z_1 and Z_2, respectively. Depending on the kind of connection and on the definition of in and out points, a specific formula can be applied in order to combine the impedances and derive the representation of the composed system.

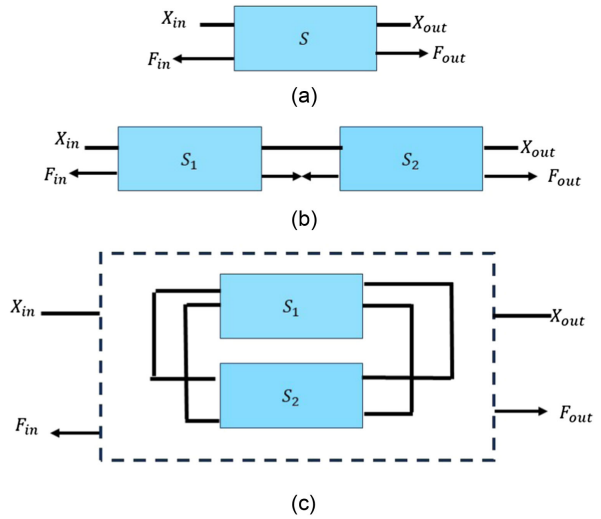

FIG. 15. Graphical representation of mechanical systems described by an impedance S (a) and their elementary connections: series (b) and parallel (c).

The simplest connection is the series connection shown in Fig. 15(b): the input of the composed system is the input of S_1; the output of the composed system is the output of S_2; the output of S_1 and the input of S_2 are coincident, with no additional force present in the connection. The total impedance Z_s of the system is

$$Z_s = Z_2 Z_1 \tag{A4}$$

The parallel connection is shown in Fig. 15(c). In this case, S_1 and S_2 have the same in and out, which define also in and out of the composed system. The total impedance $Z_{||}$ of the system is

$$Z_{||} = \begin{pmatrix} A_{||} & B_{||} \\ C_{||} & D_{||} \end{pmatrix} \tag{A5}$$

Where $A_{||}$,$B_{||}$,$C_{||}$,$D_{||}$ are calculated as follows:

$$A_{||} = A_1 + B_1 \cdot (B_1 + B_2)^{-1} \cdot (A_2 - A_1) \tag{A6}$$

$$B_{||} = B_1 \cdot (B_1 + B_2)^{-1} \cdot B_2 \tag{A7}$$

$$C_{||} = C_1 + C_2 \cdot (D_1 - D_2) \cdot (B_1 + B_2)^{-1} \cdot (A_2 - A_1) \tag{A8}$$

$$D_{||} = D_1 + (D_2 - D_1) \cdot (B_1 + B_2)^{-1} \cdot B_1 \tag{A9}$$

Another typical situation to consider is when two systems are connected similarly to a series connection, but with different definitions for in and out. One of the two is placed in the middle where the two systems are connected. This is known as connection in derivation. Here two cases are described:

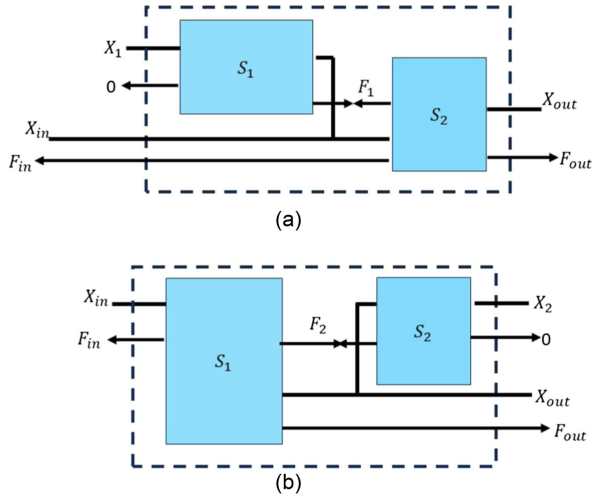

FIG. 16. Graphical representation of the connection in derivation of two mechanical systems: derivation in input (a) and derivation in output (b).

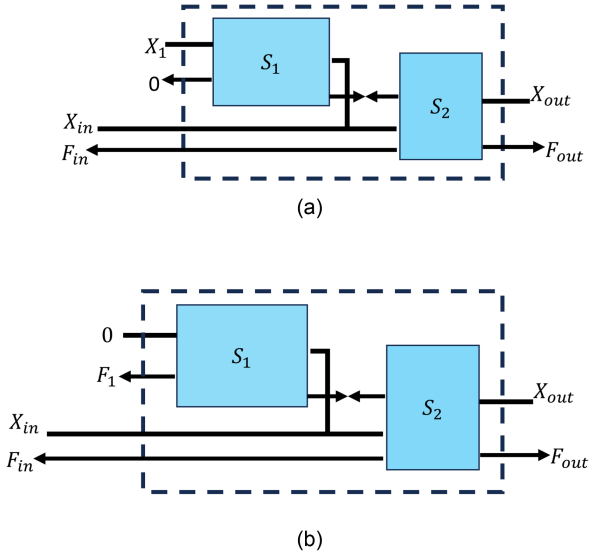

FIG. 17. Example of connections of two mechanical system in floating derivation (a) and derivation to ground (b).

(i) in and out are the same as for S_2 [derivation in input—Fig. 16(a)]

$$Z_{d,\text{in}} = Z_2 Z_1^d \tag{A10}$$

(ii) in and out are the same as for S_1 [derivation in output—Fig. 16(b)]

$$Z_{d,\text{out}} = Z_2^d Z_1 \tag{A11}$$

For both the connections in derivation, a constraint needs to be imposed to the free side, in order to define uniquely Z^d:

(i) derivation to ground—in the free side, $X = 0$ [see Fig. 17(b)]

$$Z^d = \begin{pmatrix} I & 0 \\ D_d B_d^{-1} & I \end{pmatrix} \tag{A12}$$

(ii) floating derivation—in the free side, $F = 0$ [see Fig. 17(a)]

$$Z^d = \begin{pmatrix} I & 0 \\ D_d^{-1} C_d & I \end{pmatrix} \tag{A13}$$

2. Mechanical transfer functions

The description of a mechanical system in terms of impedance matrix allows to compute the relationship between an external disturbance (for instance, a force applied to one point) and the response of the system (for instance, the vibration obtained in another point, eventually coincident with the first). This is a frequency-dependent matrix $6X6$, generically defined as transfer function (TF). In order to evaluate this operator, we need to generate the impedance connecting the application point of the force (defined as input) to the point where the effect is evaluated (defined as output). In the specific case, the other possible external force, applied to the out, must be assumed to be equal to zero.

Applying this constraint to the general equation (1), the relationship $TF(F_i, X_o)|_{F_o=0}$ between F_i and X_o can be expressed as

$$X_o = (B - AC^{-1}D)F_i \tag{A14}$$

When the algebraic identities [Eq. (A2)] can be applied, the expression can be reduced as

$$TF(F_i, X_o)|_{F_o=0} = -(C^T)^{-1} \tag{A15}$$

which is more precise at computational level, in case of very large impedance.

In the same conditions, assuming that the external force in input can generate also a vibration X_i in the application point, the transfer function from X_i to X_o has the expression

$$X_o = (A - BD^{-1}C)X_i \tag{A16}$$

which is reduced as

$$TF(X_i, X_o)|_{F_o=0} = (D^T)^{-1} \tag{A17}$$

Another transfer function of interest is the one used to calculate the external force F_{EXT} required to lock one point (out) of the system, knowing the vibration of another point (in). From the impedance connecting the two points, imposing the constraint $X_o = 0$, the following expression is obtained:

$$F_{\text{EXT}} = (-C + DB^{-1}A)X_i \quad F_{\text{EXT}} = -F_o \tag{A18}$$

which can be usually reduced as

$$TF(X_i, F_{\text{EXT}})|_{X_o=0} = (B^T)^{-1} \tag{A19}$$

In the same conditions, assuming that the external force in input can also generate a vibration X_i at the application point, the transfer function from X_i to X_o is expressed as follows

$$F_{\text{EXT}} = (-D + CA^{-1}B) \quad F_i F_{\text{EXT}} = -F_o \tag{A20}$$

which can be usually reduced as

$$TF(F_i, F_{\text{EXT}})|_{X_o=0} = -(A^T)^{-1}. \tag{A21}$$

The equation expressed in Eq. (A19) addresses the question of how the system reacts at a fixed point when another point is moved. To fully characterise the elasticity of the system, another quantity needs to be defined: the ratio between force and displacement at the same point (out) when the locked point (in) is different

$$TF(X_o, F_o)|_{X_i=0} = DB^{-1} \tag{A22}$$

In elementary elastic systems, these two quantities are equal and define what is commonly referred to as stiffness. However, in complex systems, they can be different.

APPENDIX B: CONFIGURING A MODEL: BLOCK DIAGRAM

In order to build a model of seismic isolation system and obtain from the code a full characterization of its mechanical properties, the distribution of massive and elastic elements needs to be identified and described in a proper block diagram. Each rigid body, namely its center of mass, constitute a *node* of the diagram, as in Fig. 18. Displacements, rotations, forces, and torques associated to each node constitute the dynamical variable treated by the model. Each node needs to be associated to one and only one elastic element (*link*), responsible for supporting the weight of the linked body and the ones suspended below them. The system can be modeled if, for each link, the relative impedance matrix can be computed as a function of its physical quantities, available in the code library.

Complex links, constituted by more than one elastic element, are widely used to build a seismic isolation system. For the most important ones, proper functions have been developed in order to reduce them to a single link and have their impedance available. The code can be easily updated in case new functions describing links need to added to the library.

If the system can be broken down in interconnected blocks, a simple configuration file can be built on the basis of that layout. The code will be able to automatically compute the total impedance seen between whatever pair of nodes, and compute whatever transfer function.

The code accepts additional links between pairs of nodes, to be inserted at the end of the configuration, as the whole layout of nodes has been defined. In such a way, important elements like electrical cables and control systems can be added.

There is some limitation in the disposition of those links: they cannot support weight and they cannot cross each other. Moreover, nodes which are *bypassed* in a parallel connection with an additional link become no more visible by the code: the impedance from or to those nodes cannot be computed automatically anymore. A customized formula can be inserted by the user in order to replace the automatic computation.

1. Modeling the SA

In Fig. 19, the physical layout of the SA is reported in the left side; the correspondent Octopus block scheme is shown in the right side. Each node of the scheme represents a mechanical element of the system (such as a test mass, marionette, or standard filter) connected to each other by elastic links (such as wires and inverted pendulums). In the block scheme the actuation points at the bottom stage (payload level) and the inertial sensor at the top stage are also included, each one represented by their own node.

Referring to Fig. 19, Node 1 (N_1) is defined as the test mass suspended by four fused silica wires at the next stage. The second node (N_2) is made up by the marionette and a maraging wire. Next to the marionette, there is F7. In addition to being the link between the payload and the filter chain of the SA, it is important to remind that F7 is also the mechanical structure on which the actuators at the marionette and mirror levels are bolted, and therefore this piece of information must be included in the model to correctly simulate the behavior of the SA. To achieve this, three new chains can be opened below F7, each representing an additional node in which to include information about the positions of the actuators (ACT_{MI-F7}, ACT_{MA-F7}, ACT_{F7-GR}). Nodes N_3, N_4, and N_5 store the coordinates of the actuation point with respect to the upper node. Node 6 is the rigid body associated to the complex cage described

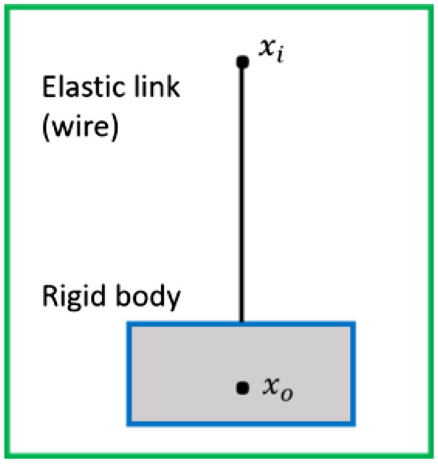

FIG. 18. Example of Octopus node.

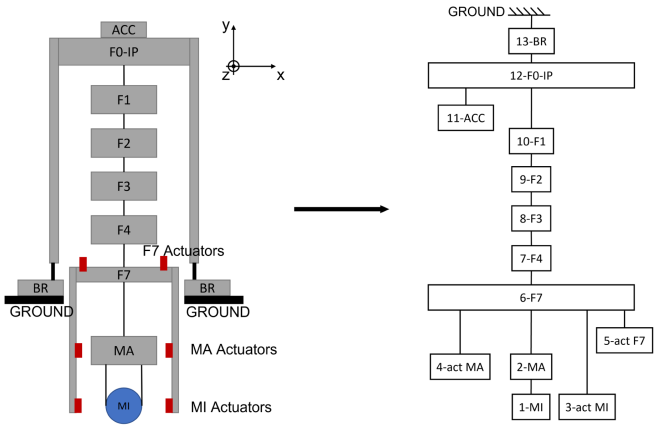

FIG. 19. Complete block scheme of the SA, including the actuation points and the inertial sensor. A total number of 13 nodes are listed from bottom to top.

above, together with its suspending wire. It is connected in series to node 7, which includes filter 4 and a suspending wire. To complete the chain of filters from filter 3 to filter 1, three additional nodes (N8, N9, N10) need to be defined. Each of these nodes consists of a standard filter and a suspending wire. Node 10 is connected in series to node 12 (Inverted pendulum), which is connected to node 13 (bottom ring) and directly connected to the ground. Node 11, the accelerometer, starts a new chain hanged below node 12.

APPENDIX C: FEEDBACK CONTROL LOOP IMPLEMENTATION

When referring to a control loop, the hardware of the system, which is composed of sensing and driving devices, needs to be considered. The sensor and the actuator can be represented as nodes occupying a well defined position. The third hardware element defining a linear control is the analog or digital device computing a correction proportional to the measured displacement, which is converted to a force by the actuator. This is the same behavior of a spring and can be implemented as the corresponding impedance [Eq. (6)] connecting the two nodes (Fig. 20, left side). The stiffness k of this virtual spring is a frequency dependent function represented by the model of the controller in frequency domain, eventually including the response of the sensor and the actuator.

The described scheme represents a linear control in the simple case, where the relative displacement between the two points is converted to an internal force applied between the same two points. Actually, other control schemes needs to be represented to cover the complexity of a control system like the one used in a seismic isolation system. For instance, the relative displacement of two bodies can be used to control just one of the two, sending no force to the second. This is what happens when an accelerometer is used for an inertial control. In other cases, the force is not sent to the body which needs to be sensed and controlled, but to a different body. This is the case of the so called *hierarchical control* of the test mass: the control force is splitted among actuators placed at different stages of the suspension in order to better exploit the actuation dynamic and reduce the control noise. In order to represent a control by an impedance matrix in any possible case, the concept of spring needs to be generalized. Let us consider the relationship

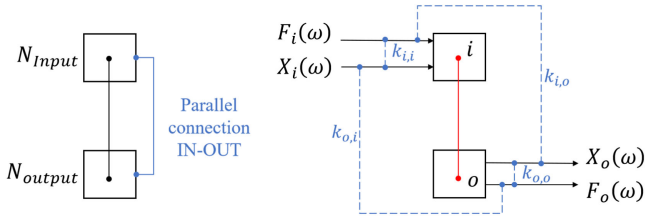

FIG. 20. Block scheme of the connection introducing a control loop.

$$\begin{cases} F_i = k_{ii} \cdot X_i - k_{io} \cdot X_o \\ F_o = k_{oi} \cdot X_i - k_{oo} \cdot X_o \end{cases} \tag{C1}$$

in which the forces applied to two nodes are related to the displacement of each node through the definition of four proportionality coefficients, according to the scheme on the right side of Fig. 20.

In order to derive the equation of the impedance matrix to be inserted in the block scheme, we start from the previous equation and solve it such that to obtain a relationship in the form where the elements A, B, C, and D can be recognized. Thus, the final set of equations is as follows:

$$\begin{aligned} X_o &= \frac{k_{ii}}{k_{io}} \cdot X_i - \frac{1}{k_{io}} \cdot F_i \\ F_o &= \left(\frac{-k_{oo} \cdot k_{ii}}{k_{io}} + k_{oi} \right) \cdot X_i + \left(\frac{k_{oo}}{k_{io}} \right) \cdot F_i \end{aligned} \tag{C2}$$

that, rewritten from scalar to matrix form, it becomes

$$\begin{pmatrix} X_o \\ F_o \end{pmatrix} = \begin{pmatrix} (K_{io}^{-1} \cdot K_{ii}) & -K_{io}^{-1} \\ (-K_{oo} \cdot K_{io}^{-1} \cdot K_{ii} + K_{oi}) & (K_{oo} \cdot K_{io}^{-1}) \end{pmatrix} \begin{pmatrix} X_i \\ F_i \end{pmatrix} \tag{C3}$$

$$A(k(\omega)) = (K_{io}^{-1} \cdot K_{ii}) \tag{C4}$$

$$B(k(\omega)) = -K_{io}^{-1} \tag{C5}$$

$$C(k(\omega)) = (-K_{oo} \cdot K_{io}^{-1} \cdot K_{ii} + K_{oi}) \tag{C6}$$

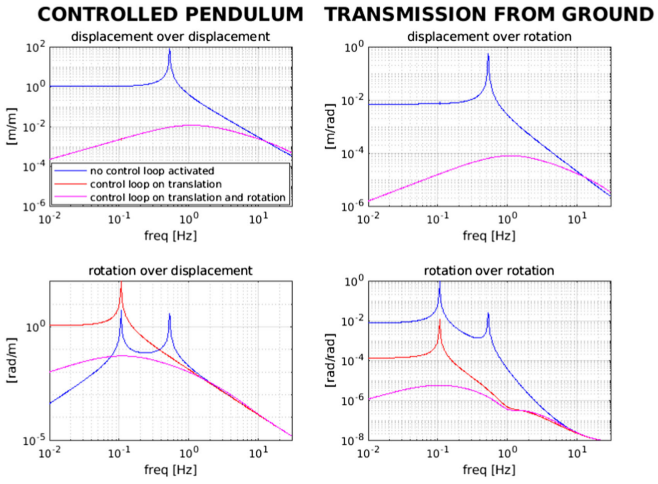

FIG. 21. Transfer function of displacement/rotation from ground to suspended mass for the simple pendulum presented in Sec. III C. The blue trace refers to the case of uncontrolled system. The red trace refers to the system controlled on longitudinal coordinate. The magenta trace refers to the system controlled on both longitudinal and angular coordinates. The implemented controls are PID with unitary gain frequency at 10 Hz for the longitudinal case and 1 Hz for the angular case.

$$D(k(\omega)) = (K_{oo} \cdot K_{io}^{-1}) \tag{C7}$$

Depending on the architecture of the control that needs to be implemented, the relationship of Eq. (C3) can be conveniently adapted to derive the specific control impedance matrix. For example, the impedance representing an inertial control is obtained assuming the two output force coefficients k_{oi} and k_{oo} are equal to zero and the two input force coefficients k_{ii} and k_{io} are equal to each other. Instead, the impedance representing a hierarchical control has only k_{io} different from zero.

1. Modeling a controlled pendulum

A simple implementation of controls has been applied to the configuration of the pendulum described in Sec. III C. Two single input-single output controls have been added, one for each degree of freedom. The feedback force and torque are applied from ground to the suspended mass; sensors of absolute translation and rotation are considered as error signals, representing in such a way something similar to the control of a cavity length and alignment, actually used in the GW detector. The transmission of the ground motion to the suspended body is shown in Fig. 21, under three different conditions:

(i) no control loop activated;
(ii) only the translation is controlled;
(iii) both controls are activated.

The model is able to predict an interesting effect, such as the impact of longitudinal control on the stability in rotation of the controlled mass. The element (2, 1) of the transfer matrix, which represents the transfer function from ground translation to body rotation, increases with the angular resonance and at lower frequency, because the longitudinal feedback force also exerts a torque on the body.

[1] P. R. Saulson, *Fundamentals of Interferometric Gravitational Wave Detectors*, 2nd ed. (World Scientific, Singapore, 2017).
[2] F. Acernese *et al.* (Virgo Collaboration), Advanced Virgo: A second-generation interferometric gravitational wave detector, Classical Quantum Gravity **32**, 024001 (2015).
[3] T. Accadia *et al.*, The seismic superattenuators of the Virgo gravitational waves interferometer, J. Low Freq. Noise Vib. Active Control **30**, 63 (2011).
[4] A. Freise, Finesse: An interferometer simulation, http://www.gwoptics.org/finesse.
[5] G. Vajente, Fast modal simulation of paraxial optical systems: The MIST open source toolbox, Classical Quantum Gravity **30**, 075014 (2013).
[6] J. Degallaix, OSCAR a Matlab based optical FFT code, J. Phys. Conf. Ser. **228**, 012021 (2010).
[7] H. Yamamoto, Sis (stationary interferometer simulation) manual, LIGO note ligo-t070039-v8, 2013, https://dcc.ligo.org/public/0000/T070039/008/SISManual-v8.pdf.
[8] S. Braccini *et al.*, Measurement of the seismic attenuation performance of the Virgo superattenuator, Astropart. Phys. **23**, 557 (2005).
[9] P. Ruggi, L'attenuazione del rumore sismico nel rivelatore di onde gravitazionale Virgo, Master's thesis, Università di Pisa, 2003.
[10] M. Punturo *et al.* (ET Collaboration), The Einstein Telescope: A third-generation gravitational wave observatory, Classical Quantum Gravity **27**, 194002 (2010).
[11] P. Ruggi *et al.*, Code related to the article: Mechanical simulation tool based on impedance matrices, 10.5281/zenodo.14981531 (2025).
[12] G. Cella and A. Vicerè (private communication).
[13] *Proceedings of the International Summer School on Experimental Physics of Gravitational Waves, Urbino, Italy, 1999*, edited by M. Barone (World Scientific, Singapore, 1999), pp. 349–378.
[14] L. D. Landau, L. P. Pitaevskii, E. M. Lifshitz, and A. M. Kosevich, *Theory of Elasticity*, 3rd ed. (Butterworth-Heinemann, 1986).
[15] H. B. Callen and T. A. Welton, Irreversibility and generalized noise, Phys. Rev. **83**, 34 (1951).
[16] G. I. Gonzàlez and P. R. Saulson, Brownian motion of a mass suspended by an anelastic wire, J. Acoust. Soc. Am. **96**, 207 (1994).
[17] S. Braccini *et al.*, Mechanical filters for the gravitational waves detector Virgo: Performance of a two-stage suspension, Rev. Sci. Instrum. **68**, 3904 (1997).
[18] G. Losurdo *et al.*, An inverted pendulum preisolator stage for the Virgo suspension system, Rev. Sci. Instrum. **70**, 2507 (1999).
[19] L. Trozzo, Low frequency optimization and performance of Advanced Virgo seismic isolation system, Ph.D. thesis, University of Siena, 2018.
[20] G. Losurdo, Ultra-low frequency inverted pendulum for the Virgo test mass suspension, Ph.D. thesis, Scuola Normale Superiore di Pisa, 1998.
[21] G. Losurdo *et al.*, Inertial control of the mirror suspensions of the Virgo interferometer for gravitational wave detection, Rev. Sci. Instrum. **72**, 3653 (2001).